HHS Public Access

Author manuscript

Nat Nanotechnol. Author manuscript; available in PMC 2022 May 18.

Published in final edited form as:

Nat Nanotechnol. 2022 January ; 17(1): 86–97. doi:10.1038/s41565-021-00997-y.

Supramolecular Arrangement of Protein in Nanoparticle Structures Predicts Nanoparticle Tropism for Neutrophils in Acute Lung Inflammation

Jacob W. Myerson[*,1], **Priyal N. Patel**[*,1], **Kathryn M. Rubey**[*,2], **Marco E. Zamora**[1], **Michael H. Zaleski**[1], **Nahal Habibi**[3], **Landis R. Walsh**[1], **Yi-Wei Lee**[4], **David C. Luther**[4], **Laura T. Ferguson**[1,5], **Oscar A. Marcos-Contreras**[1], **Patrick M. Glassman**[1], **Liudmila L. Mazaleuskaya**[1,6], **Ian Johnston**[1], **Elizabeth D. Hood**[1], **Tea Shuvaeva**[1], **Jichuan Wu**[1], **Hong-Ying Zhang**[1], **Jason V. Gregory**[3], **Raisa Y. Kiseleva**[1], **Jia Nong**[1], **Tilo Grosser**[1,6], **Colin F. Greineder**[1], **Samir Mitragotri**[7], **George S. Worthen**[2], **Vincent M. Rotello**[4], **Joerg Lahann**[3], **Vladimir R. Muzykantov**[1], **Jacob S. Brenner**[1,5]

[1]Department of Systems Pharmacology and Translational Therapeutics, Perelman School of Medicine, University of Pennsylvania

[2]Department of Pediatrics, Perelman School of Medicine, University of Pennsylvania

[3]Biointerfaces Institute and Department of Chemical Engineering, University of Michigan at Ann Arbor

[4]Department of Chemistry, University of Massachusetts at Amherst

[5]Pulmonary, Allergy, and Critical Care Division, Department of Medicine, Perelman School of Medicine, University of Pennsylvania

[6]Institute for Translational Medicine and Therapeutics, Perelman School of Medicine, University of Pennsylvania

[7]John A Paulson School of Engineering & Applied Sciences and Wyss Institute, Harvard University

Abstract

Address correspondence to: jacob.brenner@pennmedicine.upenn.edu.

Author Contributions Statement

J.W.M, P.N.P, N.H., L.R.W., D.C.L, Y.L., O.A.M., E.D.H., T.S., J.V.G., and J.N. designed and prepared nanoparticles used in the study. J.W.M., P.M.G., and R.Y.K. prepared *E. coli* for tracing in mice. J.W.M., P.N.P., L.R.W., O.A.M., L.L.M., P.M.G., I.J., J.N., and C.F.G. performed studies tracing nanoparticles in mice. J.W.M., P.N.P., M.H.Z., M.E.Z., J.W., and H.Z. performed studies of therapeutic efficacy. J.W.M., P.N.P., and L.T.F. performed studies tracing nanoparticles in human lungs. J.W.M., L.T.F. and K.M.R. performed studies tracing nanoparticle uptake in isolated cells. J.W.M., P.N.P., V.R.M., and J.S.B. analyzed all data. The manuscript was written through contributions of all authors. All authors have given approval to the final version of the manuscript.

*These authors contributed equally

Competing Interests Statement

Findings in this study contributed to United States provisional patent application number 62/943469, with J.W.M., P.N.P., L.R.W., V.R.M., and J.S.B. as inventors. The remaining authors declare no competing interests.

Code Availability

Linear discriminant and principal components analysis were completed with Gnu Octave 6.1.0 scripts adapted from https://www.bytefish.de/blog/pca_lda_with_gnu_octave/ and available in full in the supplementary materials.

This study shows that supramolecular arrangement of proteins in nanoparticle structure predicts nanoparticle accumulation in neutrophils in acute lung inflammation (ALI). We observed homing to inflamed lungs for a variety of **n**anoparticles with **a**gglutinated **p**rotein (NAPs), defined by arrangement of protein in or on the nanoparticles via; a) hydrophobic interactions; b) crosslinking; c) electrostatic interactions. Nanoparticles with symmetric protein arrangement (*e.g.*, viral capsids) had no selectivity for inflamed lungs. Flow cytometry and immunohistochemistry showed NAPs have tropism for pulmonary neutrophils. Protein-conjugated liposomes were engineered to recapitulate NAP tropism for pulmonary neutrophils. NAP uptake in neutrophils was shown to depend on complement opsonization. We; a) demonstrate diagnostic imaging of ALI with NAPs; b) show NAP tropism for inflamed human donor lungs; c) show NAPs can remediate pulmonary edema in ALI. This work demonstrates structure-dependent tropism for neutrophils drives NAPs to inflamed lungs and shows NAPs can detect and treat ALI.

Neutrophils are “first responder” cells in acute inflammation, rapidly “marginating” in and adhering to inflamed vessels.[1–7] Neutrophils can be activated by a variety of pathogen- and damage-associated factors, such as bacterial lipopolysaccharides (LPS).[8,9] In acute inflammation, neutrophils marginate in most organs, but by far most avidly in the lung capillaries. There, abundant narrow vessels provide an ideal setting for neutrophil accumulation by adhesion and by mechanical retention aided by changes in neutrophil stiffness during inflammation.[5,6,10–15] Neutrophils are therefore key cell types in acute lung inflammation (ALI). In ALI, marginated neutrophils can secrete tissue-damaging substances (proteases, reactive oxygen species) and extravasate into alveoli, leading to disrupted endothelial barrier and accumulation of neutrophils and edema in the alveoli (Figure 1a).[6,7,10–12,16] Patients suffering the worst outcomes in COVID-19 have elevated neutrophil counts and neutrophilic infiltration in the alveoli.[17–19]

One of the challenges to treating ALI with drugs is poor tolerance of side effects in patients with the severe and heterogeneous system-wide maladies that can lead to ALI.[20–23] Targeted nanoparticle delivery to marginated neutrophils could provide treatment with lessened side effects, but delivery to marginated neutrophils remains an open challenge. Antibodies against Ly6G have achieved targeting to neutrophils in mice, but also deplete circulating neutrophils.[24–27] Additionally, while Ly6G marks neutrophils in mice, there is no analogous specific and ubiquitous marker on human neutrophils.[24] Therefore, antibody targeting has not been widely adopted for targeted drug delivery to neutrophils.[26] As another route to neutrophil targeting, previous studies observed activated neutrophils take up denatured and crosslinked albumin, concluding that *denatured* protein is critical in neutrophil-nanoparticle interactions.[28,29]

Nanoparticle structural properties like shape, size, and surface charge can define targeting behaviors.[30–34] Here, we screened a diverse panel of nanoparticles to identify structural properties that predict nanoparticle uptake in pulmonary marginated neutrophils in ALI. We identified >10 nanoparticles with high selectivity for inflamed over naïve lungs. Flow cytometry and immunohistochemistry showed these nanoparticles homing to marginated neutrophils. In many of the nanoparticles we tested, proteins were arranged at the supramolecular scale by different engineered intermolecular interactions or by evolved

highly symmetrical arrangement of proteins (*e.g.*, viral capsids). Each nanoparticle with selectivity for inflamed lungs had structures with *agglutinated* protein in or on the nanoparticle. *Nanoparticles with agglutinated protein* (NAPs) are defined here as nanoparticles with supramolecular arrangement of protein in or on the nanoparticles determined by; a) hydrophobic interactions; b) non-site-specific crosslinking; c) electrostatic interactions. In contrast to NAPs, we found that viral capsids and ferritin nanocages, defined by *regularly spaced and symmetric* protein arrangement, have no selectivity for inflamed lungs. This study therefore shows that supramolecular arrangement of protein in nanoparticle structure predicts nanoparticle uptake in neutrophils in ALI. Our findings show that NAPs may improve diagnosis and treatment of acute lung inflammation.

Main

Injury-Selective Uptake of Nanoparticles in Marginated Neutrophils

Tracing of radiolabeled anti-Ly6G antibody, flow cytometry data, and histology showed intravenous (IV) LPS challenge in mice induces neutrophil margination in pulmonary vasculature 5 hours after LPS administration (Supplementary Figures 1–2). Following IV-LPS, tracing of radiolabeled, fixed, and inactivated *E. coli* indicated marginated neutrophils in the lungs taking up the bacteria (Supplementary Figure 3). To identify parameters in nanoparticle structure that correlate with nanoparticle uptake in marginated neutrophils in inflamed lungs, we thus conducted an *in vivo* screen of biodistributions for a diverse array of radiolabeled nanoparticles in naïve and IV-LPS-challenged mice. To show the radiotracer screen measures nanoparticle uptake in pulmonary marginated neutrophils, we more fully characterized *in vivo* behavior of two early hits in the screen.

Lysozyme-dextran nanogels (NGs) and poly(ethylene)glycol (PEG)-crosslinked albumin nanoparticles (albumin NPs) have been characterized as targeted drug delivery agents.[35–38] ^{125}I-labeled NGs (136.4±3.6 nm diameter, 0.10±0.02 PDI, zeta potential −0.3±0.1 mV, Supplementary Figure 4a) and human albumin NPs (317.8±3.6 nm diameter, 0.14±0.05 PDI, zeta potential −13.6±0.6 mV, Supplementary Figure 4b) were traced 30 minutes after IV injection in naïve and IV-LPS-injured mice. Absolute NG lung uptake and lung:liver ratio increased 25-fold between naïve and LPS-injured animals (Figure 1b, Supplementary Table 2). Lung uptake of human albumin NPs increased 14-fold (Figure 1c, Supplementary Table 2). Pharmacokinetics studies showed that NG uptake in inflamed lungs peaked 30 minutes after injection, followed by clearance over 24 hours (Supplementary Figure 5).

Flow cytometry identified cell types taking up fluorescent NGs or albumin NPs in the lungs. Flow data showed the total number of lung cells containing NGs or albumin NPs increased between naïve and LPS-injured lungs, corroborating radiotracer findings (Supplementary Figures 5–6). Neutrophils accounted for the bulk of NG and albumin nanoparticle accumulation in IV-LPS-injured lungs (Figures 1d–e). More than 70% of neutrophils contained nanoparticles in LPS-affected lungs, compared to <20% in naïve lungs. Likewise, more than 70% of nanoparticle uptake in the lungs was accounted for by uptake in neutrophils (Figure 1f–i, Supplementary Table 3). Leukocytes in general accounted for more than 90% of nanoparticle uptake (Supplementary Figure 6c–d). Histology of

LPS-injured lungs confirmed NGs localization to neutrophils in lung vasculature (Figure 1j). Slices in confocal images indicated NGs were inside neutrophils (Figure 1k). Intravital imaging of injured lungs showed real-time colocalizing of NGs with leukocytes in injured lungs (Figure 1l, Supplementary Movie 1).

NGs accumulated in neutrophils in other models. Radiolabeled NGs also accumulated in the lungs following intratracheal (IT)[39] and footpad LPS administration.[40] Lung:liver NG uptake ratio increased 45-fold following IT-LPS injury (Supplementary Figure 8). Footpad LPS induced an 11-fold increase in NG lung uptake 6 hours after insult and a 38-fold increase at 24 hours (Supplementary Figure 9). Footpad LPS also enhanced NG uptake in the legs. Intraplantar complete Freund's adjuvant (CFA) injection was used to induce acute neutrophil accumulation local to the footpad, rather than the lungs.[41,42] CFA injury led to a threefold increase in NG uptake in the ipsilateral paw, but no change in lung uptake (Supplementary Figure 10). Flow cytometry showed that ~90% of NG uptake in the feet was in leukocytes. CFA induced a fourfold increase in the proportion of NG uptake accounted for by neutrophils, demonstrating NG tropism for neutrophils outside of the lungs (Supplementary Figure 11).

In Vivo Screen of Diverse Nanoparticle Structures in Acutely Inflamed Lungs

We screened biodistributions of nanoparticles with different sizes, shapes, compositions, and surface charges in naïve and IV-LPS-challenged mice. A subset of these nanoparticles had structures incorporating protein, including variant NGs (nanoparticles based on hydrophobic interactions between proteins), crosslinked protein nanoparticles, nanoparticles based on electrostatic interactions of charged proteins, viral capsids, and ferritin nanocages.

Nanoparticles Based on Hydrophobic Protein Interactions—Atomic force microscopy and electron microscopy studies have shown that NGs form by lysozyme-lysozyme hydrophobic interactions, arranging a protein core stabilized by a dextran shell.[35,37,43] Noting previous work implicating denatured protein as a factor in nanoparticle uptake in neutrophils,[28,29] we obtained CD spectroscopy data indicating that secondary structure of lysozyme in NGs is the same as lysozyme itself (Supplementary Figure 12a). Lysozyme and NGs were exposed to the hydrophobic probe 8-anilino-1-naphthalenesulfonic acid (ANSA),[44] demonstrating increased hydrophobicity on NGs vs. lysozyme itself (Supplementary Figure 12b). Our data are not consistent with lysozyme being denatured in NGs, but lysozyme arrangement in NGs alters accessibility of hydrophobic domains.

NG structure was varied by modifying lysozyme-dextran composition and pH at which NGs were formed.[43] NGs of diameter ~75 nm (zeta potential 7.1±0.5 mV), ~200 nm (zeta potential −0.2±0.2 mV), and ~275 nm (zeta potential −0.4±0.1 mV) were traced, adding to data above for 130 nm NGs (Supplementary Figure 4a, Supplementary Figure 13, Supplementary Table 1). All the NG variants had consistent uptake in inflamed lungs, despite size-dependent variations in NG uptake in the liver and spleen (Figure 2a, Supplementary Table 4).

Nanoparticles Based on Protein Crosslinking—Electrohydrodynamic (EHD) jetting has formed highly monodisperse PEG-crosslinked albumin micro- and nanoparticles, as

characterized in electron microscopy studies.[38,45–47] CD spectroscopy indicated albumin secondary structure was not altered in albumin NPs, while ANSA staining indicated that PEG-albumin NPs are more hydrophilic than albumin alone (Supplementary Figure 14).

We varied the geometry and protein composition of crosslinked protein nanoparticles. Human albumin nanorods (aspect ratio 3:1), bovine albumin nanoparticles (317.3±38.5 nm, PDI 0.17±0.04, zeta potential −11.2±0.5 mV), human hemoglobin nanoparticles (328.1±16.1 nm, PDI 0.08±0.01, zeta potential −6.6±0.8 mV), human transferrin nanoparticles (345.2±10.2 nm, PDI 0.12±0.004, zeta potential −5.6±0.8 mV), and chicken lysozyme nanoparticles (298.6±12.4 nm, PDI 0.06±0.01, zeta potential −0.2±0.7 mV) were traced in naïve and IV LPS-treated mice (Figure 2b, Supplementary Figure 4b, Supplementary Figure 15, Supplementary Table 1). Including human albumin NPs (Figure 1c), five of the formulations had selectivity for inflamed lungs (Supplementary Table 5). Lysozyme nanoparticles were not selective for inflamed lungs, but accumulated in both naïve and inflamed lungs in high concentrations.

Nanoparticles Based on Electrostatic Protein Interactions—Electron microscopy studies and functional assays have recently characterized nanoparticles based on interactions between charged proteins and oppositely charged polymers or gold nanoclusters.[48–50] We traced nanoparticles comprising poly(glutamate)-tagged green fluorescent protein (E-GFP) combined with arginine-gold nanoparticles (89.0±1.6 nm diameter, PDI 0.14±0.04, zeta potential −6.4 ±0.5 mV) or with poly(oxanorborneneimide) (PONI) with guanidino and tyrosyl groups (158.9±6.2 nm diameter, PDI 0.17±0.03, zeta potential 18.3±0.5 mV) (Supplementary Figure 4c, Supplementary Table 1). For PONI/E-GFP nanoparticles, PONI was labeled with ^{131}I and E-GFP was labeled with ^{125}I to trace both components of the nanoparticles. PONI/E-GFP and arginine-gold/E-GFP nanoparticles were both selective for IV-LPS-affected lungs (Figure 2c, Supplementary Figure 16). PONI and E-GFP components of PONI/E-GFP nanoparticles accumulated in inflamed lungs at similar concentrations.

Nanoparticles Based on Symmetric Protein Arrangement—Adeno-associated virus (AAV), adenovirus, and horse spleen ferritin are nanoparticles based on arrangement of protein in symmetrical structures (sizes in Supplementary Figure 4c, zeta potentials in Supplementary Table 1).[51–56] AAV serotype 8, human adenovirus, and horse spleen ferritin had no selectivity for IV-LPS-affected lungs (Figure 2d, Supplementary Figure 17, Supplementary Table 6).

Non-Protein Nanoparticles—PEGylated liposomes (103.6±8.7 nm, PDI 0.09±0.01, zeta potential −2.2±0.2 mV) were traced with ^{111}In-DOTA-lipids and carboxylate polystyrene nanoparticles were conjugated to tracer ^{125}I-IgG (230.5±2.8 nm, PDI 0.14±0.0, zeta potential −4.0±0.8 mV, Supplementary Figure 2c–d, Supplementary Table 1). As example nanoparticles with few or no proteins, these two nanoparticles did not home to IV-LPS-affected lungs (Figure 2e, Supplementary Figure 18).

Free Protein Controls—As compared to nanoparticles based on bovine albumin, hen lysozyme, and human transferrin, albumin, lysozyme, and transferrin themselves did

not home to or have selectivity for IV-LPS-affected lungs (Supplementary Figure 19, Supplementary Table 7).

Protein-Conjugated Liposomes—Beyond data with PEGylated liposomes above, we traced protein-conjugated liposomes in naïve and IV-LPS-treated mice. Liposomes were functionalized with rat IgG conjugated via SATA-maleimide chemistry (178.8±6.9 nm, PDI 0.23±0.03, zeta potential −2.1±0.5 mV) or via click chemistry methods (128.3±4.3 nm, PDI 0.17±0.03, zeta potential −4.1±0.2 mV), in which IgG was conjugated to dibenzocyclooctyne (DBCO) and the modified IgG was conjugated to azide-liposomes (Figure 3a, Supplementary Figure 4d, Supplementary Table 1).[57] Compared to bare and SATA-IgG liposomes, DBCO-IgG liposomes had enhanced tropism for IV-LPS-affected lungs (Figure 3b, Supplementary Figure 20, Supplementary Table 8). IT-LPS injury also enhanced lung uptake of DBCO-IgG liposomes (Supplementary Figure 21). Flow cytometry with fluorescent DBCO-IgG liposomes confirmed liposome tropism for neutrophils in inflamed lungs (Figure 3c–d, Supplementary Figure 22). ~90% of liposome signal in inflamed lungs was in neutrophils and >98% was in leukocytes.

We confirmed that DBCO modification of IgG confers neutrophil tropism on IgG-liposomes by titrating the DBCO:IgG ratio (Supplementary Figure 4d for liposome sizes, Supplementary Figure 23, Supplementary Table 1 for liposome zeta potentials). Results in Figure 3b used 20 DBCO per IgG. Reducing DBCO:IgG reduced DBCO-IgG liposome uptake in IV-LPS-affected lungs (Figure 3e, Supplementary Table 9). DBCO-IgG itself did not accumulate in the lungs (Supplementary Figure 24), showing that incorporation of the modified protein in nanoparticle structure was necessary for inflamed lung tropism. CD spectroscopy indicated DBCO did not change IgG secondary structure (Supplementary Figure 25).

In the above data, nanoparticles based on “agglutination” of protein (NAPs) in hydrophobic interactions, crosslinking, and charge interactions all exhibited selectivity for inflamed lungs (Figure 2a–c), with additional data indicating that this selectivity is based on tropism for marginated neutrophils (Figure 1). Adding hydrophobic DBCO to protein on liposomes led to liposome uptake in neutrophils in inflamed lungs (Figure 3), indicating hydrophobic interactions between proteins on liposome surfaces also predict tropism for marginated neutrophils. Nanoparticles based on highly symmetrical protein arrangement had no tropism for inflamed lungs (Figure 2d). NAP selectivity for inflamed lungs did not linearly correlate with size or zeta potential (Supplementary Figure 26), accommodated both spheres and rods, and was observed with eight different types of protein. Agglutinated protein was unique as a structural motif common to all nanoparticles with high selectivity for inflamed lungs. Principal component and linear discriminant analyses of our compiled biodistributions confirmed; a) NAPs as nanoparticles with tropism for inflamed lungs; b) alignment of DBCO-IgG liposomes with other NAPs (Supplementary Figures 27–28).

Complement Opsonization as a Mechanism in NAP Tropism for Neutrophils

We conducted *in vitro* and *in vivo* studies isolating biological mechanisms by which neutrophils recognize NAPs. Exposure of NGs to serum prior to *in vitro* incubation with

neutrophils led to a >30-fold increase in NG uptake (Figure 4a, Supplementary Figure 29a–b). We hypothesized that serum opsonins are a determinant in NG interactions with neutrophils. Mass spectrometry quantified the abundance of different proteins adsorbed on NGs after incubation in serum, identifying large quantities of complement proteins C3 and C5 (Figure 4b, Supplementary Figure 30a). C3 and C5 were significantly more abundant than complement C2 and C4, signifying predominance of alternative pathway complement activation.[58]

Serum was heat treated to inactivate complement.[59] Heat treatment eliminated the effect of serum on NG uptake in neutrophils (Figure 4c, Supplementary Figure 29a–b). Cobra venom factor (CVF) treatment to deplete serum complement by C3 activation[60] also eliminated serum effects on NG-neutrophil interactions (Figure 4c, Supplementary Figure 29a–b). Serum from a mouse treated with CVF yielded identical results (Supplementary Figure 29a–b). *In vitro*, LPS stimulation of neutrophils did not modify NG uptake (Figure 4d, Supplementary Figure 29c–d). *In vitro*, complement interactions with NAPs, rather than LPS stimulation of neutrophils, determined NAP uptake in neutrophils.

We treated mice with intraperitoneal CVF to deplete complement *in vivo* prior to NAP administration. CVF treatment reduced NG tropism for IV-LPS-inflamed lungs by >50%, with >5-fold reduction in lungs:blood ratio (Figure 4e, Supplementary Figure 31).

We also performed mass spectrometry analysis of serum proteins on adenovirus capsids, a protein nanoparticle with no tropism for neutrophils in inflamed lungs. All tested complement proteins were reduced on adenovirus vs. NGs, with C5 and factor B absent on adenovirus (Figure 4f, Supplementary Figure 30a–c). CVF treating serum reduced the quantities of C3 and factor B on NGs, and levels of these proteins on adenovirus capsid with naïve serum were less than those on NGs with complement-depleted serum (Supplementary Figure 30c).

Imaging Lung Inflammation with NAPs

Computerized tomography (CT) imaging can diagnose ALI by detecting pulmonary edema, but cannot distinguish ALI from cardiogenic pulmonary edema (CPE).[61] CPE was induced in mice via propranolol infusion.[62] CT imaging confirmed pulmonary edema after propranolol infusion (Figure 5a–b, Supplementary Figure 32, Supplementary Movies 2 and 3). NGs homed to IV-LPS-affected lungs, but not CPE-affected lungs (Figure 5c). We tested NGs as SPECT-CT contrast agents for ALI by imaging ^{111}In-labeled NGs (Supplementary Figure 33) in naïve and IV-LPS-affected lungs. ^{111}In SPECT signal was detectable in LPS-affected lungs, but at background level in naïve lungs (Figure 5d, Supplementary Movies 4–7). Previous studies have noted the potential for diagnostic imaging of lung inflammation based on neutrophils, including clinical data with autologous neutrophils in ALI and chronic obstructive pulmonary disease.[12,63] However, our results with NAPs are the first use of nanoparticles with tropism for neutrophils for non-invasive imaging of inflamed lungs with a translational modality.

NAP Accumulation in Inflamed Human Lungs Ex Vivo

We performed experiments to test NAP tropism for inflamed human lungs. NGs were added to single cell suspensions prepared from human lungs. NGs accumulated in leukocytes in the suspensions in a dose-dependent manner (Supplementary Figure 34a–b). Fluorescent or ^{125}I-labeled NGs were infused via arterial catheter into *ex vivo* human lungs excluded from transplant due to lung damage.[64] Tissue dye indicated areas of the lungs perfused by NG suspensions (Supplementary Figure 34c). For fluorescent NG experiments, high- and low-perfusion regions were selected for histology. NGs were detectable only in well-perfused tissue (Supplementary Figure 34d). In experiments with ^{125}I-NGs, ^{131}I-ferritin was concurrently infused as a control particle without tropism for injured mouse lungs. NGs retained in human lungs at >5-fold higher concentration than ferritin (Supplementary Figure 34e). NGs were concentrated in highly-perfused lung regions, while ferritin was uniformly distributed (Supplementary Figure 35). Our data indicate NAP tropism for neutrophils in inflamed mouse lungs may be recapitulated in human lungs.

Effects of NAPs in Acute Lung Inflammation

Mice were treated with nebulized LPS as a high-throughput model for severe acute respiratory distress syndrome (ARDS).[65] Histology showed nebulized LPS caused hemorrhage and airway infiltration by neutrophils 24 hours after insult (Supplementary Figure 36). In bronchoalveolar lavage fluid (BALF), nebulized LPS elevated neutrophil/leukocyte concentrations 50-fold and protein concentration 3-fold (Figure 6a–b, Supplementary Figure 37), indicating vascular disruption and edema.

DBCO-IgG liposomes, NGs, and bare liposomes were administered (30 mg/kg dose) two hours after nebulized LPS. BALF leukocytes and protein were reduced by >50% by DBCO-IgG liposomes, but were unaffected by bare liposomes and NGs (Figure 6a–b, Supplementary Figure 37). DBCO-IgG liposome effects on BALF leukocytes and protein were dose-dependent, with IC50s of 5.7 mg/kg and 1.5 mg/kg, respectively (Figure 6c–d, Supplementary Figure 38). CXCL2, a chemoattractant in neutrophil diapedesis,[66] was elevated in BALF and liver by nebulized LPS. BALF and liver CXCL2 were reduced by DBCO-IgG liposomes (Figure 6e, Supplementary Figure 39). Cytokine IL-6 is elevated in plasma in severe ARDS.[67] In our model, DBCO-IgG liposomes suppressed plasma IL-6 in a dose-dependent manner (Supplementary Figure 40).

DBCO-IgG liposomes suppressed neutrophil accumulation in BALF in a manner consistent with suppression of BALF leukocytes (Figure 6f, Supplementary Figure 41). Quantifying *intravascular* neutrophils via radiotracer Ly6G antibody, we found DBCO-IgG liposomes reduced pulmonary marginated neutrophils, increased circulating neutrophils, and transiently increased spleen neutrophils, relative to untreated values (Figure 6g, Supplementary Figure 42). Complete blood count (CBC) confirmed DBCO-IgG liposome effects on circulating neutrophils (Figure 6h, Supplementary Figure 43). CBC also indicated DBCO-IgG liposomes mitigate LPS suppression of lymphocytes and platelets and have insignificant effects on red blood cells (Supplementary Figures 43–44).

These findings indicate DBCO-IgG liposomes cause neutrophils to leave the lungs, getting sequestered in the spleen or returning to circulation. Accordingly, we observe lower neutrophil extravasation into alveoli and less edema after DBCO-IgG liposome treatment (Figure 6i). DBCO-IgG liposomes had no significant effects on body weight (Supplementary Figure 45), but changes to signaling molecules CXCL2 and IL-6 and effects on platelets and lymphocytes indicate systemic effects for these NAPs.

Conclusions

This study identifies nanoparticle properties leading to tropism for neutrophils in inflamed lungs. These neutrophils take up *nanoparticles with agglutinated protein* (NAPs), but not nanoparticles whose surface proteins are arranged with regular and symmetric spacing (*e.g.*, viral capsids and protein nanocages[51,53–56]). “Agglutination” is defined here by the three types of protein-protein interactions enumerated in figure 2, which are designed without specific supramolecular arrangement. Electron microscopy data confirms there is no symmetry or regularity in protein-protein spacing in NAPs[35,37,43,46,47,49,50]. Thus, the structures of nanoparticles tested in our studies are differentiated by arrangement of protein at the supramolecular scale: Nanoparticles with or without regular spacing and symmetry in protein arrangement. Differences in nanoparticle tropism for neutrophils in inflamed lungs aligned with differences in supramolecular-scale protein arrangement, but not differences in size, shape, or zeta potential (Supplementary Figures 26–28). Correlation between this type of supramolecular structure and immune cell tropism has not previously been reported.

Supporting our conclusions, we re-engineered liposomes to behave like NAPs. We hypothesized that addition of the hydrophobic molecule DBCO to IgG on liposomes would recapitulate protein “agglutination” seen in NAPs based on hydrophobic interactions. Three lines of data confirm this: DBCO-IgG liposomes and NGs have similar tropism for neutrophils in inflamed lungs; replacing DBCO with less hydrophobic SATA-maleimide conjugation[68] abrogates neutrophil tropism; titrating down the amount of DBCO on IgG ratchets down neutrophil tropism of DBCO-IgG liposomes.

We showed the mechanism by which neutrophils recognize NAPs is dependent on complement opsonization. While prior literature shows the importance of complement opsonization in nanoparticle uptake[69], our observations are unique in suggesting that the alternative pathway of complement responds to differences in supramolecular arrangement of protein.

Finally, we showed that some NAPs have anti-inflammatory properties. DBCO-IgG liposomes, without any cargo drug, provide dose-dependent reduction in protein and leukocyte extravasation into pulmonary alveoli in a model of the human lung disease ARDS. Neutrophil tracing showed that DBCO-IgG liposomes effect these benefits by decreasing; neutrophils’ retention in inflamed pulmonary vasculature; neutrophils’ ability to cross the pulmonary vascular barrier. DBCO-IgG liposomes decreased systemic and local inflammatory cytokines and chemokines, which may indicate effects on other cell types (*e.g.*, CXCL2 is secreted primarily by monocytes and macrophages)[66,70]. These anti-inflammatory effects may be viewed as side effects, since they imply effects on multiple cell

types and signaling molecules (A full discussion of immunological implications is included in the supplementary materials). Not all NAPs have anti-inflammatory effects (*e.g.*, NGs), so NAPs may be loaded with drugs, such as antibiotics, that have benefits in ALI.

In conclusion, supramolecular arrangement of protein in nanoparticle structure predicts nanoparticle uptake in pulmonary marginated neutrophils during acute inflammation. *Agglutinated protein* is a motif in nanoparticle structure correlated with nanoparticle tropism for neutrophils. The NAPs identified in this study and future NAPs based on parameters outlined here could be untapped resources for diagnosis and treatment of devastating inflammatory disorders like ALI.

Methods

Nanoparticle Synthesis

NGs, crosslinked protein nanoparticles, charged protein nanoparticles, liposomes, and polystyrene nanoparticles were prepared as previously described.[36,43] Details of synthesis for each type of nanoparticle are included in the supplementary material. Nanoparticles, proteins, and bacteria were labeled with ^{125}I, ^{131}I, or ^{111}In according to described methods.[57] Details of labeling techniques are provided in the supplement.

E. Coli Preparation

TOP10 *E. coli* (ThermoFisher #C404002) were grown overnight in Terrific broth with ampicillin. Bacteria were heat-inactivated by 20-minute incubation at 60°C, then fixed by overnight incubation in 4% paraformaldehyde. After fixation, bacteria were pelleted by centrifugation at 1000xg for 10 minutes. Pelleted bacteria were washed three times in PBS, prior to resuspension by pipetting. Bacterial concentration was verified by optical density at 600 nm, prior to radiolabeling as described above. Bacteria were administered IV in mice (7.5×10^7 colony forming units in a 100 μL suspension per mouse).

Nanoparticle and Protein Tracing in Mice

Nanoparticle or protein biodistributions were tested by IV injecting nanoparticles or protein (suspended to 100 μL in phosphate buffered saline (PBS) or 0.9% saline at a dose of 2.5 mg/kg with tracer quantities of radiolabeled material) in C57BL/6 male mice from Jackson Laboratories. For experiments tracing anti-Ly6G biodistributions to locate intravascular neutrophils, radiolabeled anti-Ly6G was administered IV at 0.1 mg/kg. Quantity of injected radioactivity was measured by gamma counter (Perkin-Elmer) immediately before injection. To determine nanoparticles masses for dosing; NGs and charged protein nanoparticles were prepared from reactants at known concentrations in synthetic methods involving no material loss; crosslinked protein nanoparticles were re-suspended from weighed powder; polystyrene nanoparticles, ferritin, and viral capsids were purchased at known concentrations. Liposomes were prepared from reactants at known concentrations and previous work with the same synthetic methods assessed low material losses during filtration and purification of liposomes.[57,71]

Biodistributions in naïve mice were compared to biodistributions in injury models. Biodistribution data were collected at 30 minutes after nanoparticle or protein injection, unless otherwise stated. Blood was collected by vena cava draw and mice were sacrificed by exsanguination and cervical dislocation. Organs were harvested and rinsed in saline, and blood and organs were examined for nanoparticle or protein retention by gamma counter. To calculate concentration in organs, quantity of retained radioactivity was normalized to organ weights.

For IV LPS, mice were anesthetized with 3% isoflurane before retroorbital injection of LPS from *E. coli* strain B4 at 2 mg/kg in 100 μL PBS. After five hours, mice were anesthetized with ketamine-xylazine (10 mg/kg ketamine, 100 mg/kg xylazine, intramuscular administration) and before jugular vein nanoparticle or protein injection. For IT LPS, B4 LPS was administered to mice (anesthetized with ketamine/xylazine) at 1 mg/kg in 50 μL of PBS via tracheal catheter, followed by 100 μL of air.[71] NGs were injected 16 hours after IT LPS and DBCO-IgG liposomes were injected 1, 2, or 6 hours after IT LPS. For footpad LPS, B4 LPS was administered at 1 mg/kg in 50 μL PBS via footpad injection. NGs were injected IV 6 or 24 hours after footpad LPS. For cardiogenic pulmonary edema, mice were anesthetized with ketamine/xylazine and administered propranolol in saline (3 μg/mL) via jugular vein catheter at 83 μL/min over 120 minutes[62] prior to IV NG injection. For localized footpad inflammation, mice were anesthetized with 3% isoflurane and 20 μL of CFA or 20 μL of sham saline was injected subcutaneously in the central plantar region of the left hind paw,[42] six hours before IV NG injection.

Single Cell Suspension Flow Cytometry

Single cell suspensions were prepared from male C57BL/6 mouse lungs for flow cytometry. Fluorescent nanoparticles were administered at 2.5 mg/kg 30 minutes prior to sacrifice and lung extraction. Mice were anesthetized with ketamine/xylazine (10 mg/kg ketamine, 100 mg/kg xylazine, intramuscular administration) prior to installation of tracheal catheter secured by suture. After sacrifice by vena cava exsanguination, lungs were perfused by right ventricle with ~10 mL of cold PBS. Lungs were then infused via tracheal catheter with 1 mL of cold PBS solution with 5 U/mL dispase, 2.5 mg/mL collagenase I, and 1 mg/mL of DNAse I. Immediately after infusion, the trachea was sutured shut while removing the tracheal catheter. Lungs with intact trachea were removed via thoracotomy and kept on ice prior to manual disaggregation.

Single cell suspensions were also prepared from mouse feet. Feet were removed immediately following sacrifice by cervical dislocation and 100 μL of dispase/collagenase/DNAse was injected subcutaneously in the feet. Tissue was separated from the bones while the feet were held in 1 mL of dispase/collagenase/DNAse.

Disaggregated lung or foot tissue was aspirated in an additional 2 mL of dispase/collagenase/DNAse and incubated at 37°C for 45 minutes, vortexing every 10 minutes. After addition of 1 mL of fetal calf serum, tissue suspensions were strained through 100 μm filters and centrifuged 400xg for 5 minutes. Pelleted material was resuspended in 10 mL of cold ACK lysing buffer. The resulting suspensions were strained through 40 μm filter, incubated for 10 minutes on ice, and centrifuged 400xg for 5 minutes. The pelleted material was rinsed

in 10 mL of FACS buffer (2% fetal calf serum and 1 mM EDTA in PBS). After 400xg/5 minute centrifugation, pellets were resuspended in 2% PFA in 1 mL FACS buffer for 10 minutes room temperature incubation. Fixed cell suspensions were centrifuged 400xg for 5 minutes and resuspended in 1 mL of FACS buffer.

To stain fixed cells, 100 μL aliquots of cell suspensions were pelleted 400xg for 5 minutes, then resuspended in labeled antibody diluted in FACS buffer (1:150 dilution for anti-Ly6G, APC-anti-CD31, or PE-anti-F480 antibodies and 1:500 dilution for anti-CD45 andtibodies). Samples were incubated with staining antibodies for 20 minutes at room temperature in the dark, diluted with 1 mL of FACS buffer, and pelleted at 400xg for 5 minutes. Stained pellets were resuspended in 200 μL of FACS buffer immediately prior to flow cytometry (BD Accuri). Data was gated to exclude debris and doublets. Controls with no stain, obtained from naïve and IV-LPS-injured mice, established gates for negative/positive staining with FITC/AlexFluor 488, PE, PerCP/Cy5.5, and APC/AlexaFluor 647. Single stain controls allowed automatic generation of compensation matrices in FCS Express software.

To analyze intravascular leukocyte populations in lungs, mice received IV FITC-anti-CD45 five minutes prior to sacrifice. Populations of intravascular vs. extravascular leukocytes were assessed by also staining fixed cell suspensions with PerCP-conjugated anti-CD45 and/or Alexa Fluor 647-conjugated anti-Ly6G. Comparing PerCP anti-CD45 with FITC anti-CD45 signal indicated intravascular vs. extravascular leukocytes. Comparison of Alexa Fluor 647 anti-Ly6G, PerCP anti-CD45, and FITC anti-CD45 signal indicated intravascular vs. extravascular neutrophils.

To characterize nanoparticle distribution among different cells in lungs or feet, fluorescent nanoparticles were administered at 2.5 mg/kg via jugular vein injection and circulated for 30 minutes. Fixed single cell suspensions were stained and coincidence of nanoparticle fluorescence with anti-CD45, anti-Ly6G, PE anti-CD31, or PE anti-F480 fluorescence was assessed.

In Vitro Neutrophil Uptake of Nanoparticles

Bone marrow was collected from pooled femorae of C57BL/6 mice. Neutrophils were isolated with StemCell Technologies RoboSep Mouse Neutrophil Enrichment Kit by magnetic bead-mediated depletion of non-neutrophils. To serum-treat NGs prior to incubation with neutrophils, 5×10^9 FITC-labeled NGs in 10 μL PBS were incubated with 10 μL serum for one hour at 37°C. 1×10^6 neutrophils were rotated with 5×10^9 NGs in 20μL PBS for 15 minutes at 37°C. For flow cytometry (BD Accuri C6), neutrophils were washed and stained with PerCP/Cy5.5 Ly6G antibodies (BD Biosciences, 1:100 dilution) and non-neutrophils were excluded from analysis via Ly6G staining (see Supplementary Figure 27 for gating). NG fluorescence in neutrophils was quantified.

To probe the role of complement in neutrophil-nanoparticle interactions, complement was depleted from serum via two methods: heat treatment and cobra venom factor (CVF). For heat treatment, serum was incubated at 56°C for one hour and denatured proteins were removed by centrifugation at 10,000g for 15 minutes. For CVF treatment, 10 units CVF per mL serum were incubated one hour at 37°C, then centrifuged 10,000g for 15 minutes.

Nanoparticle incubation with heat- and CVF-treated serum followed the same protocol described above for naïve serum.

In Vivo Effects of Complement on Nanoparticle Tropism for Neutrophils

Mice were dosed with 100 μg/kg CVF via intraperitoneal injection 24 hours prior to NG administration or blood draw to test *in vivo* effects of complement depletion on nanoparticle-neutrophil interactions. For experiments with both LPS and CVF, B4 LPS from *E. coli* was administered IV at 2 mg/kg 19 hours after CVF and five hours before IV NGs (2.5 mg/kg), as described in Nanoparticle and Protein Tracing in Mice.

Mass Spectrometry Profiles of Protein Coronae on Nanoparticles

25 μL NGs or adenovirus capsids in a 5 mg/mL suspension were incubated with equivalent volume of wild type or CVF-treated (as above) mouse serum or saline sham for one hour at 37°C. Nanoparticles were pelleted by centrifugation and washed with 1 mL PBS three times to separate from unbound serum proteins.

Opsonized and sham-opsonized nanoparticles were prepared for mass spectrometry analysis as follows: Samples were solubilized and digested with the iST kit (PreOmics GmbH) per manufacturer protocol. Nanoparticle pellets were re-suspended, reduced, and alykylated by addition of sodium deoxycholate (SDC) buffer containing tris(2-carboxyethyl)phosphine (TCEP) and 2-chloroacetamide. The resulting suspensions were heated at 95°C for 10 minutes. Proteins were enzymatically hydrolyzed for 1.5 hours at 37°C by endoproteinase Lys-C and trypsin. The resulting peptides were de-salted, dried by vacuum centrifugation, and reconstituted in 0.1% trifluoroacetic acid (TFA) containing indexed retention time (iRT) peptides (Biognosys Schlieren). UPLC-mass spectrometry data were obtained and analyzed by published methods,[72,73] as detailed in the supplement.

SPECT/CT Imaging

Imaging techniques, as described previously,[57] are detailed in the supplement. SPECT and CT data, in NIFTI format, were opened with ImageJ software (FIJI package) and processed for background removal, pseudo-color assignment, and three-dimensional reconstruction, as detailed in the supplement.

Nanoparticle Administration in Human Lungs

Human lungs were obtained after organ harvest from transplant donors whose lungs were in advance deemed unsuitable for transplantation. Lungs were kept at 4°C and used within 24 hours of organ harvest. Lungs were inflated with low pressure oxygen and oxygen flow was maintained at 0.8 L/min for gentle inflation. Pulmonary artery subsegmental branches were endovascularly cannulated, then tested for retrograde flow by perfusing for 5 minutes with Steen solution containing a small amount of green tissue dye at 25 cm H_2O pressure. Pulmonary veins through which efflux of perfusate emerged were noted, allowing collection of solutions after passage through the lungs. A 2 mL mixture of ^{125}I-labeled NGs and ^{131}I-labeled ferritin was injected through the arterial catheter. ~100mL of 3% BSA in PBS was passed through the same catheter to rinse unbound nanoparticles. A solution of green tissue dye was subsequently injected through the same catheter. The cannulated lung lobe

was dissected into ~1 g segments, which were evaluated for density of tissue dye staining. Segments were weighed, divided into ‘high’, ‘medium’, ‘low’, and ‘null’ levels of dye staining, and measured for ^{131}I and ^{125}I signal in a gamma counter.

For experiments with cell suspensions derived from human lungs (chosen for research use as above), single cell suspensions were generously provided by Edward Morrisey at the University of Pennsylvania. Aliquots of 600,000 cells were pelleted at 400xg for 5 minutes and resuspended in 100 μL FACs buffer containing different quantities of FITC-dextran NGs. Cells and NGs were incubated at room temperature for 60 minutes before two-fold pelleting at 400xg with 1 mL PBS washes. Cells were re-suspended in 200 μL FACS buffer for staining with APC anti-human CD45 (1:500 dilution, 20-minute room temperature incubation). Cells were pelleted at 400xg for 5 minutes and resuspended in 200 μL PBS for immediate analysis with flow cytometry (BD Accuri). Negative/positive NG or anti-CD45 signal was established by comparison to unstained cells. Single-stained controls indicated no spectral overlap between FITC-NG fluorescence and anti-CD45 APC fluorescence.

Effects of Nanoparticles in Nebulized LPS Model

Mice were exposed to nebulized B4 LPS in a whole-body exposure chamber, with separate compartments for each mouse (MPC-3 AERO; Braintree Scientific). To maintain adequate hydration, mice were injected with 1 mL sterile saline warmed to 37°C, intraperitoneally, immediately before LPS exposure. LPS was reconstituted in PBS to 10 mg/mL and stored at −80°C until use. Immediately before nebulization, LPS was thawed and diluted to 5 mg/mL with PBS. 5 mL of diluted LPS was aerosolized via a jet nebulizer connected to the exposure chamber (NEB-MED H, Braintree Scientific). Nebulization was performed until all liquid was nebulized (~20 minutes).

DBCO-IgG liposomes (20:1 DBCO:IgG, 2.5, 5,10, or 30 mg/kg dose), bare liposomes (30 mg/kg dose), NGs (30 mg/kg dose), or saline sham were administered via retro-orbital injections of 100 μL of suspension 2 hours after LPS exposure. Mice were anesthetized with 3% isoflurane to facilitate injections. Blood draws and BALF were collected 24 hours after LPS exposure, as previously described and detailed in the supplement.[71] Mice were weighed before administration of nebulized LPS and before BALF and blood draws.

To stain for flow cytometry, BALF samples were centrifuged at 300xg for 4 minutes, the supernatant was aspirated, and 100 μL of staining buffer (1:1000 APC-anti-CD45 or 1:150 Alexa Fluor 488-anti-Ly6G in FACS buffer) was added. Samples were stained for 30 minutes at room temperature in the dark, then 1 mL of FACS buffer was added, samples were centrifuged at 300xg for 4 minutes, and supernatant was aspirated. Cells were resuspended in 900 μL of FACS buffer for flow cytometry analysis (BD Accuri). Forward scatter (area) vs. side scatter (area) plots gated out non-cellular debris and forward scatter (area) vs. forward scatter (height) plots gated out doublets. Unstained controls set gates for APC and Alexa Fluor 488 signal. Single-stained controls showed no spectral overlap between APC-anti-CD45 and Alexa Fluor 488-anti-Ly6G. CD45- and Ly6G-positive cells determined leukocyte and neutrophil concentrations, respectively.

To trace intravascular neutrophils after nebulized LPS treatment and 10 mg/kg DBCO-IgG liposome dosing, ^{125}I-anti-Ly6G (0.1 mg/kg) was administered 1 or 22 hours after liposomes, and biodistributions were determined as described above. In mice treated with DBCO-IgG liposomes, blood was drawn into EDTA via the vena cava before exsanguination. Lungs and liver were removed after obtaining BALF and stored at −80°C. Blood was immediately evaluated with CBC measurements (Abaxis VetScan HM5). Blood remaining after CBC was centrifuged at 1500xg for 10 minutes at 4°C and plasma was extracted and stored at −80°C. Chemokine CXCL2 and cytokine IL-6 were measured in BALF, plasma, and lung and liver homogenates according to published methods detailed in the supplement.[74]

Circular Dichroism Spectroscopy

Proteins were prepared in deionized and filtered water at concentrations of 0.155 mg/mL for human albumin, 0.2 mg/mL for hen lysozyme, and 0.48 mg/mL for IgG. Albumin NPs, NGs, and IgG-coated liposomes were diluted such that albumin, lysozyme, and IgG concentrations in the suspensions matched concentrations of corresponding protein solutions. Protein and nanoparticle solutions were analyzed in quartz cuvettes with 10 mm path length in an Aviv circular dichroism spectrometer. The instrument was equilibrated in nitrogen at 25°C for 30 minutes prior to use and samples were analyzed with sweeps between 185 and 285 nm in 1 nm increments. Each data point was obtained after a 0.333 s settling time, with a 2 s averaging time. CDNN[75] software deconvolved CD data (expressed in millidegrees) via neural network algorithm assessing alignment of spectra with library-determined spectra for helices, antiparallel sheets, parallel sheets, beta turns, and random coil.[75]

8-anilino-1-naphthalenesulfonic Acid Nanoparticle Staining

8-anilino-1-naphthalenesulfonic acid (ANSA) at 0.06 mg/mL was mixed with lysozyme, human albumin, or IgG at 1.5 mg/mL in PBS. For nanoparticle analysis, nanoparticle suspensions were prepared such that albumin, lysozyme, and IgG concentrations in the suspensions matched the 1.5 mg/mL concentration of protein solutions. Protein or nanoparticles and ANSA were reacted at room temperature for 30 minutes. Excess ANSA was removed from solutions by 3 centrifugations against 3 kDa cutoff centrifugal filters (Amicon). After resuspension to original volume, ANSA-stained protein/nanoparticle solutions/suspensions were examined for fluorescence (excitation 375 nm) and absorbance maxima corresponding to ANSA.

Histology

For imaging neutrophils in naïve and IV-LPS-affected lungs, mice were given IV anti-Ly6G and sacrificed 30 minutes later. Lungs were embedded in M1 medium, flash frozen, and sectioned in 10 μm slices. Sections were stained with Alexa Fluor 594-goat anti-rat secondary antibody (1:200 dilution) and imaged with epifluorescence microscopy. Similarly, rhodamine-dextran NGs were administered IV in IV-LPS mice 30 minutes prior to sacrifice. Lungs were sectioned as above and stained with clone 1A8 anti-Ly6G antibody, followed by Alexa Fluor 350-goat anti-rat secondary antibody (1:150 dilution), prior to epifluorescence and confocal imaging of NG and neutrophil fluorescence.

For histological verification of injury following nebulized LPS treatment, one set of injured mouse lungs and one set of naïve lungs was infused intratracheally with 4% paraformaldehyde. The trachea was tied off and lungs and trachea were removed via thoracotomy. The lungs were suspended in 4% paraformaldehyde for overnight fixation prior to embedding in paraffin, sectioning, and hematoxylin/eosin staining.

Sections of human lungs were obtained after administration of rhodamine-dextran NGs. NG-perfused and non-perfused tissue regions were harvested, embedded in M1 medium, flash frozen, and sectioned in 10 μm slices. NG fluorescence and tissue autofluorescence were detected with epifluorescence imaging.

Live Lung Imaging

A mouse was anesthetized with ketamine/xylazine five hours after IV LPS. A jugular vein catheter was placed for injection of NGs, anti-CD45, and fluorescent dextran. A patch of skin on the back of the mouse, around the juncture between the ribcage and the diaphragm, was denuded. The mouse was maintained on mechanical ventilation and the lungs were exposed via incision at the juncture between the ribs and the diaphragm. A coverslip affixed to a rubber o-ring was sealed to the incision by vacuum. The exposed lungs were focused under the objective using autofluorescence. With 100 ms exposure, channels corresponding to violet, green, near-red, and far-red fluorescence were sequentially imaged. Rhodamine-dextran NGs (2.5 mg/kg), Brilliant Violet-anti-CD45 (0.8 mg/kg), and Alexa Fluor 647-70 kDa dextran (40 mg/kg) were injected via jugular vein. Images were recorded for 30 minutes in SlideBook software and opened in ImageJ (FIJI distribution) for composition in movies with co-registration of the four fluorescent channels.

Animal and human study protocols

All animal studies were carried out in strict accordance with Guide for the Care and Use of Laboratory Animals as adopted by National Institute of Health and approved by University of Pennsylvania Institutional Animal Care and Use Committee (IACUC). All animal experiments used male C57BL/6J mice, 6–8 weeks old, purchased from Jackson Laboratories. Mice were maintained at 20–25°C, 50%±20% humidity, and on a 12/12 hour dark/light cycle with food and water ad libitum.

Human lungs were obtained by the University of Pennsylvania Lung Biology Institute's Human Lung Tissue Bank (HLTB) from Gift of Life Donor Program (Philadelphia, PA, United States of America). Lungs provided to the HLTB were determined unsuitable for transplantation into a recipient, and would have been discarded if not used for our studies. Lungs provided by the HLTB for these studies are de-identified and cannot be linked to individual donors. Clinical staff procuring and distributing the tissue through the HLTB are not involved in the research after distribution of the de-identified tissue. Studies employing de-identified tissue from the HLTB were therefore determined by the University of Pennsylvania Institutional Review Board (IRB) to be IRB-exempt and were not considered human subjects research as defined by the Office of Human Research Protection of the National Institutes of Health. De-identified patient data for human lungs (age, sex, and cause of death) are tabulated in Supplementary Table 11.

Statistical Analysis

Error bars indicate standard error of the mean throughout. Significance tests are described in captions. Statistical power was determined for statements of statistical significance and tabulated in the supplementary materials.

Supplementary Material

Refer to Web version on PubMed Central for supplementary material.

Acknowledgments

This research was supported by NIH R01HL125462 (V.R.M.). The authors acknowledge funding from the Defense Threat Reduction Agency (HDTRA-1-15-0045, J.L., V.R.M.). V.M.R. acknowledges NIH EB022641. J.W.M. was supported by NIH T32HL07915 while conducting this research. O.A.M. received funding from the American Heart Association (19CDA345900001). L.L.M. was supported in part by NIH UL1TR001878. Circular dichroism spectroscopy data were obtained at the University of Pennsylvania Biological Chemistry Resource Center. SPECT-CT images were obtained by Eric Blankenmyer in collaboration with the University of Pennsylvania Perelman School of Medicine Small Animal Imaging Facility. Single cell suspensions prepared from human lungs were generously provided by Edward E. Morrisey's group at the University of Pennsylvania. The authors report no competing financial interests.

Data Availability

All data supporting the findings of this study are presented graphically or in tables in the paper and supplementary materials. Raw numerical imaging, flow cytometry, gamma counter, mass spectrometry, and spectroscopy data provided graphically in this study are available as tabulated values from the corresponding author upon reasonable request.

References

1. Wright HL, Moots RJ, Bucknall RC & Edwards SW Neutrophil function in inflammation and inflammatory diseases. Rheumatology 49, 1618–1631 (2010). [PubMed: 20338884]
2. Sônego F et al. Paradoxical roles of the neutrophil in sepsis: protective and deleterious. Front. Immunol 7, 155 (2016). [PubMed: 27199981]
3. Jickling GC et al. Targeting neutrophils in ischemic stroke: translational insights from experimental studies. J. Cereb. Blood Flow Metab 35, 888–901 (2015). [PubMed: 25806703]
4. Mehta J et al. Neutrophil function in ischemic heart disease. Circulation 79, 549–556 (1989). [PubMed: 2537159]
5. Grommes J & Soehnlein O Contribution of neutrophils to acute lung injury. Mol Med 17, 293–307 (2011). [PubMed: 21046059]
6. Summers C et al. Neutrophil kinetics in health and disease. Trends Immunol. 31, 318–324 (2010). [PubMed: 20620114]
7. Gee MH & Albertine KH Neutrophil-endothelial cell interactions in the lung. Annu. Rev. Physiol 55, 227–248 (1993). [PubMed: 8466175]
8. Mayadas TN, Cullere X & Lowell CA The multifaceted functions of neutrophils. Annu. Rev. Pathol 9, 181–218 (2014). [PubMed: 24050624]
9. Mantovani A, Cassatella MA, Costantini C & Jaillon S Neutrophils in the activation and regulation of innate and adaptive immunity. Nat. Rev. Immunol 11, 519–531 (2011). [PubMed: 21785456]
10. Williams AE & Chambers RC The mercurial nature of neutrophils: still an enigma in ARDS? Am. J. Physiol. Lung Cell Mol. Physiol 306, L217–30 (2014). [PubMed: 24318116]
11. Zemans RL & Matthay MA What drives neutrophils to the alveoli in ARDS? Thorax 72, 1–3 (2017). [PubMed: 27974631]

12. Summers C et al. Pulmonary retention of primed neutrophils: a novel protective host response, which is impaired in the acute respiratory distress syndrome. Thorax 69, 623–629 (2014). [PubMed: 24706039]
13. Doerschuk CM Mechanisms of leukocyte sequestration in inflamed lungs. Microcirculation 8, 71–88 (2001). [PubMed: 11379793]
14. Worthen GS, Schwab B, Elson EL & Downey GP Mechanics of stimulated neutrophils: cell stiffening induces retention in capillaries. Science 245, 183–186 (1989). [PubMed: 2749255]
15. Kuebler WM & Goetz AE The marginated pool. Eur Surg Res 34, 92–100 (2002). [PubMed: 11867908]
16. Doyle NA et al. Neutrophil margination, sequestration, and emigration in the lungs of L-selectin-deficient mice. J. Clin. Invest 99, 526–533 (1997). [PubMed: 9022088]
17. Zhou Z et al. Heightened Innate Immune Responses in the Respiratory Tract of COVID-19 Patients. Cell Host Microbe 27, 883–890.e2 (2020). [PubMed: 32407669]
18. Zeng F et al. Can we predict the severity of coronavirus disease 2019 with a routine blood test? Pol. Arch. Intern. Med 130, 400–406 (2020). [PubMed: 32356642]
19. Wang D et al. Clinical Characteristics of 138 Hospitalized Patients With 2019 Novel Coronavirus-Infected Pneumonia in Wuhan, China. JAMA 323, 1061–1069 (2020). [PubMed: 32031570]
20. Brenner JS Nanomedicine for the Treatment of Acute Respiratory Distress Syndrome. The 2016 ATS Bear Cage Award-winning Proposal. Annals of the American Thoracic Society 14, 561–564 (2017). [PubMed: 28304180]
21. Brenner JS, Greineder C, Shuvaev V & Muzykantov V Endothelial nanomedicine for the treatment of pulmonary disease. Expert Opin Drug Deliv 12, 239–261 (2015). [PubMed: 25394760]
22. Gao Smith F et al. Effect of intravenous β−2 agonist treatment on clinical outcomes in acute respiratory distress syndrome (BALTI-2): a multicentre, randomised controlled trial. Lancet 379, 229–235 (2012). [PubMed: 22166903]
23. National Heart, Lung, and Blood Institute Acute Respiratory Distress Syndrome (ARDS) Clinical Trials Network et al. Randomized, placebo-controlled clinical trial of an aerosolized β_2-agonist for treatment of acute lung injury. Am. J. Respir. Crit. Care Med 184, 561–568 (2011). [PubMed: 21562125]
24. Lee PY, Wang J-X, Parisini E, Dascher CC & Nigrovic PA Ly6 family proteins in neutrophil biology. J. Leukoc. Biol 94, 585–594 (2013). [PubMed: 23543767]
25. Daley JM, Thomay AA, Connolly MD, Reichner JS & Albina JE Use of Ly6G-specific monoclonal antibody to deplete neutrophils in mice. J. Leukoc. Biol 83, 64–70 (2008). [PubMed: 17884993]
26. Vij N, Min T, Bodas M, Gorde A & Roy I Neutrophil targeted nano-drug delivery system for chronic obstructive lung diseases. Nanomedicine 12, 2415–2427 (2016). [PubMed: 27381067]
27. Bartneck M & Wang J Therapeutic targeting of neutrophil granulocytes in inflammatory liver disease. Front. Immunol 10, 2257 (2019). [PubMed: 31616430]
28. Wang Z, Li J, Cho J & Malik AB Prevention of vascular inflammation by nanoparticle targeting of adherent neutrophils. Nat. Nanotechnol 9, 204–210 (2014). [PubMed: 24561355]
29. Chu D, Gao J & Wang Z Neutrophil-Mediated Delivery of Therapeutic Nanoparticles across Blood Vessel Barrier for Treatment of Inflammation and Infection. ACS Nano 9, 11800–11811 (2015). [PubMed: 26516654]
30. Myerson JW et al. Non-affinity factors modulating vascular targeting of nano- and microcarriers. Adv. Drug Deliv. Rev 99, 97–112 (2016). [PubMed: 26596696]
31. Mitragotri S & Lahann J Physical approaches to biomaterial design. Nat. Mater 8, 15–23 (2009). [PubMed: 19096389]
32. Anselmo AC & Mitragotri S Impact of particle elasticity on particle-based drug delivery systems. Adv. Drug Deliv. Rev 108, 51–67 (2017). [PubMed: 26806856]
33. Ernsting MJ, Murakami M, Roy A & Li S-D Factors controlling the pharmacokinetics, biodistribution and intratumoral penetration of nanoparticles. J. Control. Release 172, 782–794 (2013). [PubMed: 24075927]

34. Anselmo AC & Mitragotri S Cell-mediated delivery of nanoparticles: taking advantage of circulatory cells to target nanoparticles. J. Control. Release 190, 531–541 (2014). [PubMed: 24747161]
35. Ferrer MCC et al. Icam-1 targeted nanogels loaded with dexamethasone alleviate pulmonary inflammation. PLoS One 9, e102329 (2014). [PubMed: 25019304]
36. Myerson JW et al. Flexible nanoparticles reach sterically obscured endothelial targets inaccessible to rigid nanoparticles. Adv. Mater. Weinheim 30, e1802373 (2018).
37. Myerson JW et al. Cross-linker-Modulated Nanogel Flexibility Correlates with Tunable Targeting to a Sterically Impeded Endothelial Marker. ACS Nano 13, 11409–11421 (2019). [PubMed: 31600053]
38. Rahmani S et al. Long-circulating Janus nanoparticles made by electrohydrodynamic co-jetting for systemic drug delivery applications. J Drug Target 23, 750–758 (2015). [PubMed: 26453170]
39. Brenner JS et al. Mechanisms that determine nanocarrier targeting to healthy versus inflamed lung regions. Nanomedicine 13, 1495–1506 (2017). [PubMed: 28065731]
40. Lu M & Munford RS The transport and inactivation kinetics of bacterial lipopolysaccharide influence its immunological potency in vivo. J. Immunol 187, 3314–3320 (2011). [PubMed: 21849675]
41. Gregory NS et al. An overview of animal models of pain: disease models and outcome measures. J. Pain 14, 1255–1269 (2013). [PubMed: 24035349]
42. Ghasemlou N, Chiu IM, Julien J-P & Woolf CJ CD11b+Ly6G- myeloid cells mediate mechanical inflammatory pain hypersensitivity. Proc. Natl. Acad. Sci. USA 112, E6808–17 (2015). [PubMed: 26598697]
43. Li J, Yu S, Yao P & Jiang M Lysozyme-dextran core-shell nanogels prepared via a green process. Langmuir 24, 3486–3492 (2008). [PubMed: 18302424]
44. Bertsch M & Kassner RJ Selective staining of proteins with hydrophobic surface sites on a native electrophoretic gel. J. Proteome Res 2, 469–475 (2003). [PubMed: 14582643]
45. Roh K, Martin DC & Lahann J Biphasic Janus particles with nanoscale anisotropy. Nat. Mater 4, 759–763 (2005). [PubMed: 16184172]
46. Gregory JV et al. Systemic brain tumor delivery of synthetic protein nanoparticles for glioblastoma therapy. Nat. Commun 11, 5687 (2020). [PubMed: 33173024]
47. Hwang S et al. Anisotropic hybrid particles based on electrohydrodynamic co-jetting of nanoparticle suspensions. Phys. Chem. Chem. Phys 12, 11894–11899 (2010). [PubMed: 20844780]
48. Lee Y et al. In Vivo Editing of Macrophages through Systemic Delivery of CRISPR-Cas9-Ribonucleoprotein-Nanoparticle Nanoassemblies. Adv. Therap 2, 1900041 (2019).
49. Mout R et al. Direct Cytosolic Delivery of CRISPR/Cas9-Ribonucleoprotein for Efficient Gene Editing. ACS Nano 11, 2452–2458 (2017). [PubMed: 28129503]
50. Lee Y-W et al. Direct Cytosolic Delivery of Proteins through Coengineering of Proteins and Polymeric Delivery Vehicles. J. Am. Chem. Soc 142, 4349–4355 (2020). [PubMed: 32049533]
51. Russo CJ & Passmore LA Electron microscopy: Ultrastable gold substrates for electron cryomicroscopy. Science 346, 1377–1380 (2014). [PubMed: 25504723]
52. Mietzsch M et al. Comparative analysis of the capsid structures of aavrh.10, aavrh.39, and AAV8. J. Virol 94, (2020).
53. Yu X et al. Cryo-EM structure of human adenovirus D26 reveals the conservation of structural organization among human adenoviruses. Sci. Adv 3, e1602670 (2017). [PubMed: 28508067]
54. Drouin LM & Agbandje-McKenna M Adeno-associated virus structural biology as a tool in vector development. Future Virol. 8, 1183–1199 (2013). [PubMed: 24533032]
55. Nemerow GR, Stewart PL & Reddy VS Structure of human adenovirus. Curr Opin Virol 2, 115–121 (2012). [PubMed: 22482707]
56. Pontillo N, Pane F, Messori L, Amoresano A & Merlino A Cisplatin encapsulation within a ferritin nanocage: a high-resolution crystallographic study. Chem. Commun 52, 4136–4139 (2016).

57. Hood ED et al. Vascular Targeting of Radiolabeled Liposomes with Bio-Orthogonally Conjugated Ligands: Single Chain Fragments Provide Higher Specificity than Antibodies. Bioconjug. Chem 29, 3626–3637 (2018). [PubMed: 30240185]
58. Dunkelberger JR & Song W-C Complement and its role in innate and adaptive immune responses. Cell Res. 20, 34–50 (2010). [PubMed: 20010915]
59. Soltis RD, Hasz D, Morris MJ & Wilson ID The effect of heat inactivation of serum on aggregation of immunoglobulins. Immunology 36, 37–45 (1979). [PubMed: 422227]
60. Haihua C, Wei W, Kun H, Yuanli L & Fei L Cobra Venom Factor-induced complement depletion protects against lung ischemia reperfusion injury through alleviating blood-air barrier damage. Sci. Rep 8, 10346 (2018). [PubMed: 29985461]
61. Saguil A & Fargo M Acute respiratory distress syndrome: diagnosis and management. Am. Fam. Physician 85, 352–358 (2012). [PubMed: 22335314]
62. Fang X et al. Novel role for CFTR in fluid absorption from the distal airspaces of the lung. J. Gen. Physiol 119, 199–207 (2002). [PubMed: 11815669]
63. Tregay N et al. Use of autologous 99mTechnetium-labelled neutrophils to quantify lung neutrophil clearance in COPD. Thorax 74, 659–666 (2019). [PubMed: 30674586]
64. Brenner JS et al. Red blood cell-hitchhiking boosts delivery of nanocarriers to chosen organs by orders of magnitude. Nat. Commun 9, 2684 (2018). [PubMed: 29992966]
65. Matute-Bello G et al. An official American Thoracic Society workshop report: features and measurements of experimental acute lung injury in animals. Am. J. Respir. Cell Mol. Biol 44, 725–738 (2011). [PubMed: 21531958]
66. De Filippo K et al. Mast cell and macrophage chemokines CXCL1/CXCL2 control the early stage of neutrophil recruitment during tissue inflammation. Blood 121, 4930–4937 (2013). [PubMed: 23645836]
67. Meduri GU et al. Persistent elevation of inflammatory cytokines predicts a poor outcome in ARDS. Plasma IL-1 beta and IL-6 levels are consistent and efficient predictors of outcome over time. Chest 107, 1062–1073 (1995). [PubMed: 7705118]
68. Duncan RJ, Weston PD & Wrigglesworth R A new reagent which may be used to introduce sulfhydryl groups into proteins, and its use in the preparation of conjugates for immunoassay. Anal. Biochem 132, 68–73 (1983). [PubMed: 6353995]
69. Szebeni J, Muggia F, Gabizon A & Barenholz Y Activation of complement by therapeutic liposomes and other lipid excipient-based therapeutic products: prediction and prevention. Adv. Drug Deliv. Rev 63, 1020–1030 (2011). [PubMed: 21787819]
70. Qin C-C, Liu Y-N, Hu Y, Yang Y & Chen Z Macrophage inflammatory protein-2 as mediator of inflammation in acute liver injury. World J. Gastroenterol 23, 3043–3052 (2017). [PubMed: 28533661]
71. Hood ED et al. Antioxidant protection by PECAM-targeted delivery of a novel NADPH-oxidase inhibitor to the endothelium in vitro and in vivo. J. Control. Release 163, 161–169 (2012). [PubMed: 22974832]
72. Nesvizhskii AI, Keller A, Kolker E & Aebersold R A statistical model for identifying proteins by tandem mass spectrometry. Anal. Chem 75, 4646–4658 (2003). [PubMed: 14632076]
73. Bielow C, Mastrobuoni G & Kempa S Proteomics quality control: quality control software for maxquant results. J. Proteome Res 15, 777–787 (2016). [PubMed: 26653327]
74. Parhiz H et al. PECAM-1 directed re-targeting of exogenous mRNA providing two orders of magnitude enhancement of vascular delivery and expression in lungs independent of apolipoprotein E-mediated uptake. J. Control. Release 291, 106–115 (2018). [PubMed: 30336167]
75. Böhm G, Muhr R & Jaenicke R Quantitative analysis of protein far UV circular dichroism spectra by neural networks. Protein Eng 5, 191–195 (1992). [PubMed: 1409538]

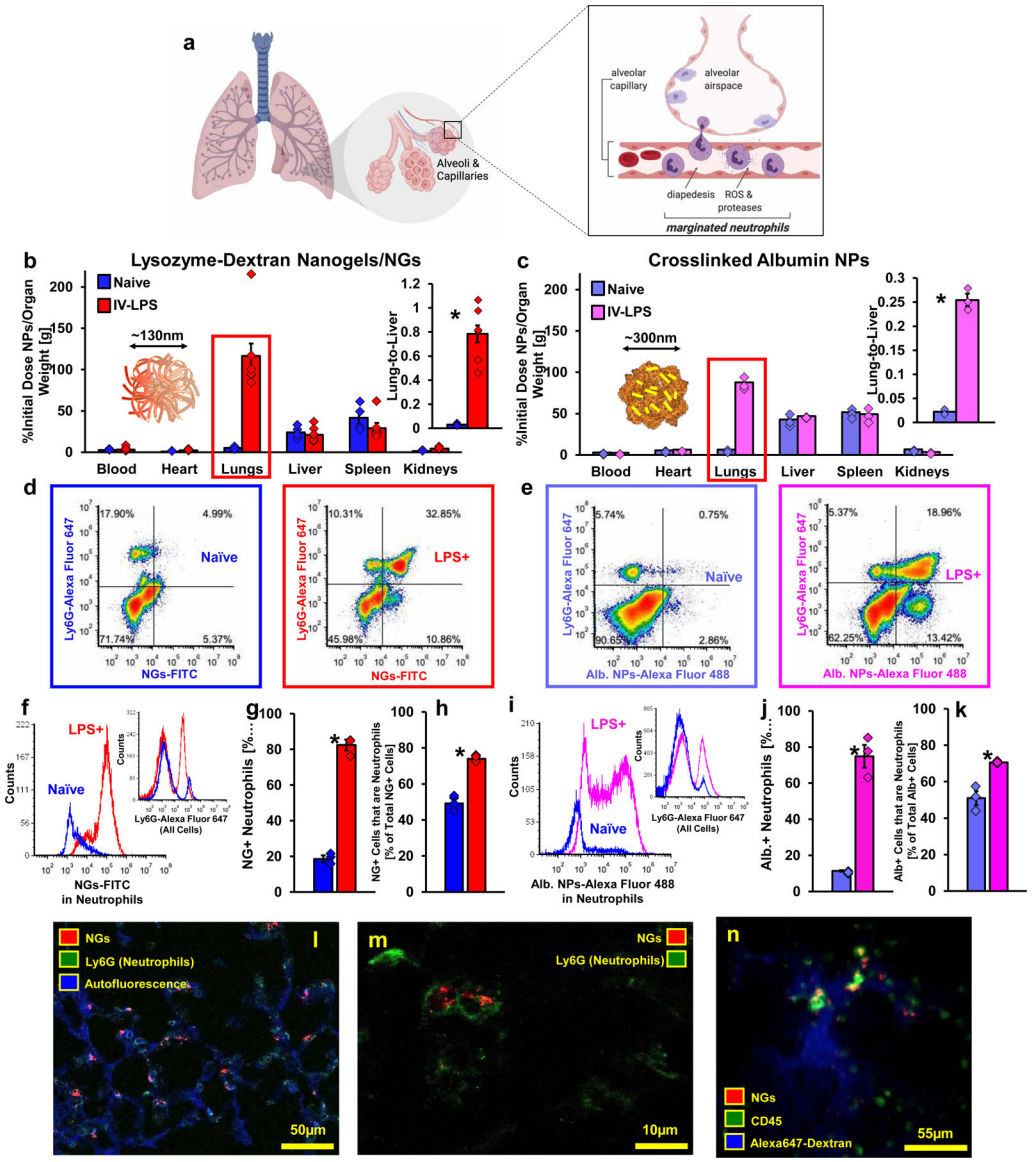

Figure 1. Lysozyme-Dextran Nanogels and Crosslinked Albumin Nanoparticles Accumulate in Marginated Neutrophils in Inflamed Lungs.

(a) Schematic of neutrophil margination and extravasation in inflamed lungs (created with BioRender.com). (b) Biodistributions of lysozyme-dextran nanogels (NGs) in naïve (n=4 animals) and IV-LPS-affected (n=8 animals) male C57BL/6 mice (*red box: $p<1\times10^{-10}$, *: $p=0.00008$*). (c) Biodistributions of PEG-NHS crosslinked human albumin nanoparticles (albumin NPs) in naïve (n=3 animals) and IV-LPS-injured (n=3 animals) mice (*red box: $p<1\times10^{-10}$, *: $p=0.004$*). (d-k) Flow cytometry characterization of single cell suspensions prepared from naïve and IV-LPS-affected mouse lungs. (d-e) Vertical axis indicates Ly6G staining for neutrophils and horizontal axis indicates signal from fluorescent NGs (d) or fluorescent albumin NPs (e). (f/h) NG/albumin NP fluorescent signal from neutrophils in IV-LPS-injured mouse lungs (red/pink), compared to naïve lungs (blue) (inset: Flow cytometry data verifying increased neutrophil concentration in IV-LPS-injured mouse lungs (red/pink). (g-h, j-k) Fraction of neutrophils positive for NGs (g) or albumin NPs (j) in

naïve or IV-LPS-injured lungs and fraction of NG-positive (h) or albumin NP-positive (k) cells that are neutrophils. For (g-h), NGs/naïve: n=4 animals, NGs/LPS: n=4 animals. For (j-k), albumin NPs/naïve: n=3 animals, albumin NPs/LPS: n=3 animals. (g)*: $p=2.6\times10^{-7}$. (h)*: $p=1.7\times10^{-5}$. (j)*: p=0.0006. (k)*: p=0.007. (l-m) Fluorescence micrographs indicating association of NGs (red) with neutrophils (green, Ly6G stain) in the lungs of an IV-LPS-affected mouse (blue, tissue autofluorescence). Data are from histology for two naïve mice and two IV-LPS affected mice. (n) Single frame from real-time intravital imaging of NG (red) uptake in leukocytes (green) in the lungs of one IV-LPS-affected mouse (blue, Alexa Fluor 647-dextran). Statistical significance in (b) and (c) is derived from two-way ANOVA with Sidak's multiple comparisons test. Statistical significance in (g), (h), (j), and (k) is derived from paired two-tailed t-tests. All error bars indicate mean ± SEM.

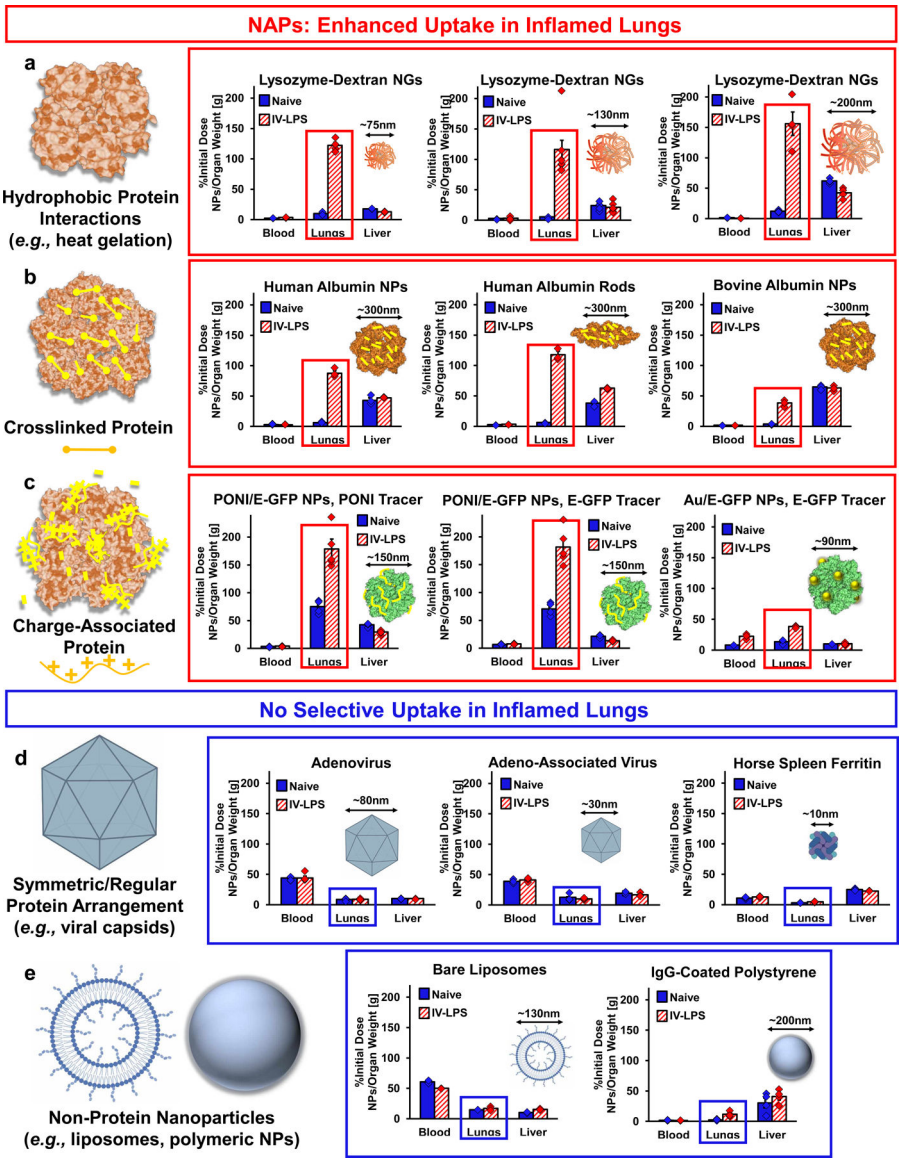

Figure 2. Screen of Diverse Nanoparticle Biodistributions in Naïve and IV-LPS-Affected Lungs.

(a-c) Nanoparticles with agglutinated protein (NAPs) accumulate in acutely inflamed lungs. (a) Biodistributions of variant NGs indicating uptake of 75 nm NGs (n=4 IV-LPS animals, n=4 naïve animals, *red box:* $p<1\times10^{-10}$) and 200 nm NGs (n=5 IV-LPS, n=5 naïve, *red box:* $p<1\times10^{-10}$) in LPS-injured lungs, but not naïve lungs. Data for 130 nm NGs is identical to that presented in figure 1b. (b) Biodistributions of variant crosslinked albumin nanoparticles indicating uptake of albumin nanorods (n=3 IV-LPS animals, n=3 naïve animals, *red box:* $p<1\times10^{-10}$) and bovine albumin nanoparticles (n=3 IV-LPS animals, n=3 naïve animals, *red box:* $p<1\times10^{-10}$) in LPS-injured, but not naïve lungs. Data for human albumin nanoparticles is identical to that presented in figure 1c. (c) Biodistributions of charge-agglutinated protein nanoparticles, indicating uptake of particles comprised of glutamate-tagged green fluorescent protein (E-GFP) and guanidine-tagged poly(oxanorborneneimide) (PONI) or particles comprised of E-GFP and guanidine-tagged gold nanoparticles (Au) in LPS-injured

(PONI: n=5 animals, Au: n=3 animals), but not naïve (PONI: n=4 animals, Au: n=3 animals) lungs. PONI/E-GFP data reflects tracing of both ^{131}I-labeled PONI and ^{125}I-labeled E-GFP. For PONI tracer data, *red box* $p<1\times10^{-10}$. For E-GFP tracer data, *red box: p=0.0003*. For Au/E-GFP data, *red box:* $p=1.6\times10^{-9}$. (d) Nanoparticles based on symmetric supramolecular arrangement of protein do not have tropism for inflamed lungs (schematics created with BioRender.com). Biodistributions of adenovirus (n=5 IV-LPS animals, n=5 naïve animals, *blue box: p=0.88*), adeno-associated virus (n=3 IV-LPS animals, n=3 naïve animals, *blue box: p=0.56*), and ferritin nanocages (n=5 IV-LPS animals, n=5 naïve animals, *blue box: p=0.35*) indicating no selectivity for LPS-injured vs. naïve lungs. (e) Biodistributions of bare liposomes (schematic created with BioRender.com, n=4 IV-LPS animals, n=4 naïve animals) indicating no selectivity for LPS-injured vs. naïve lungs (*blue box: p=0.31*). Biodistributions of IgG-coated polystyrene nanoparticles indicating low levels of uptake in both naïve (n=4 animals) and LPS-injured (n=4 animals) lungs (*blue box: p=0.0004*). Statistical significance in all panels is derived from two-way ANOVA with Sidak's multiple comparisons test. All error bars indicate mean ± SEM.

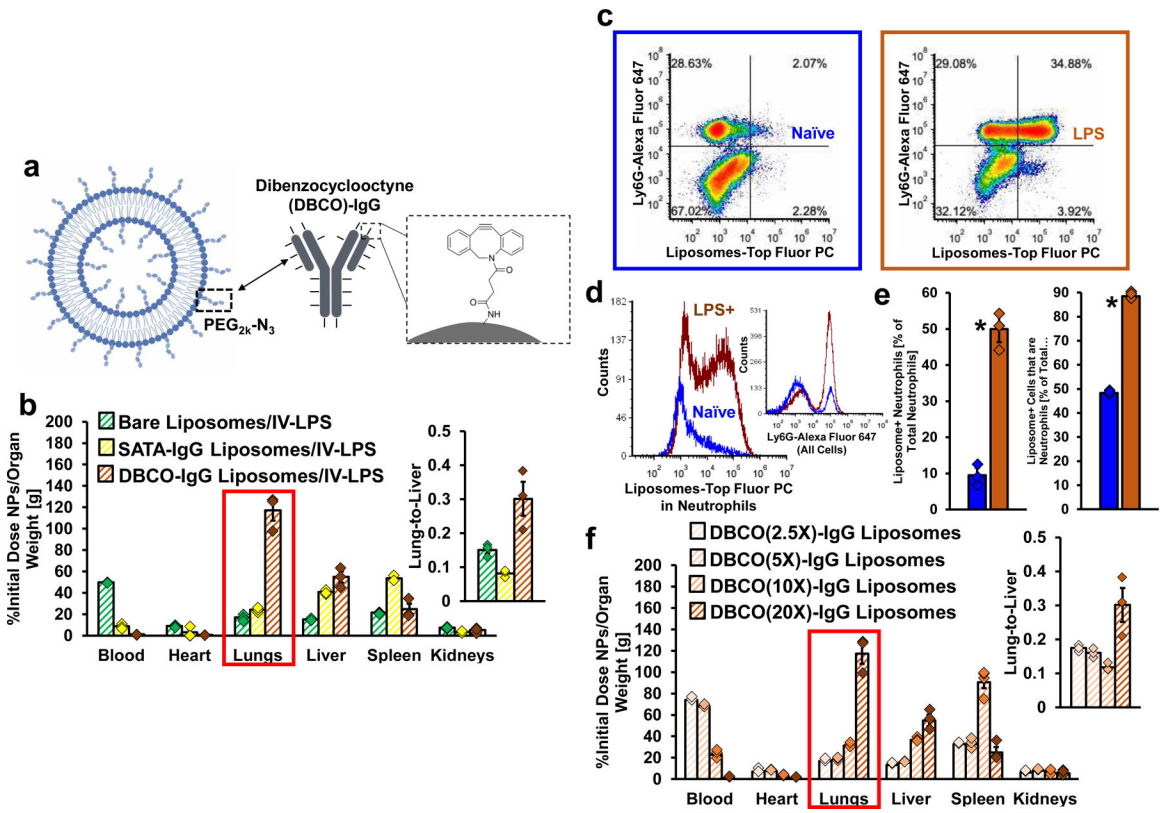

Figure 3. Engineering of Liposome Surface Chemistry to Confer NAP-like Behavior in LPS-Inflamed Lungs.

(a) Schematic of antibody-coated liposomes prepared via copper-free click reaction of azide-functionalized liposomes with dibenzocyclooctyne (DBCO)-functionalized IgG (liposome schematic created with BioRender.com). (b) Biodistributions in IV-LPS-injured mice for bare liposomes (n=3 animals), liposomes conjugated to IgG via SATA-maleimide chemistry (n=3 animals), and liposomes conjugated to IgG via DBCO-azide chemistry (n=3 animals) (*red box:* $p<1\times10^{-10}$ for DBCO-IgG liposomes vs. bare liposomes and DBCO-IgG liposomes vs. SATA-IgG liposomes). (c) Mouse lungs flow cytometry data indicating Ly6G anti-neutrophil staining density vs. levels of DBCO-IgG liposome uptake. (d) Flow cytometry data verifying increased DBCO-IgG liposome uptake in and selectivity for neutrophils following LPS insult. Inset: Verification of increased concentration of neutrophils in the lungs following LPS. (e) Fraction of neutrophils positive for DBCO-IgG liposomes in naïve (n=3 animals) or IV-LPS-injured (n=3 animals) lungs (**: $p=0.0003$*) and fraction of DBCO-IgG liposome-positive cells that are neutrophils (**: $p=1.7\times10^{-6}$*) (f) Biodistributions in IV-LPS-injured mice for azide-functionalized liposomes conjugated to IgG loaded with 2.5 (n=3 animals), 5 (n=3 animals), 10 (n=4 animals), and 20 DBCO molecules per IgG (n=3 animals, *red box:* $p<1\times10^{-10}$ for DBCO(20X)-IgG liposomes compared to each of the other DBCO density groups). Statistical significance in (b) and (f) is derived from two-way ANOVA with Tukey's multiple comparisons test. Statistical significance in (e) is derived from paired two-tailed t-tests. All error bars indicate mean ± SEM.

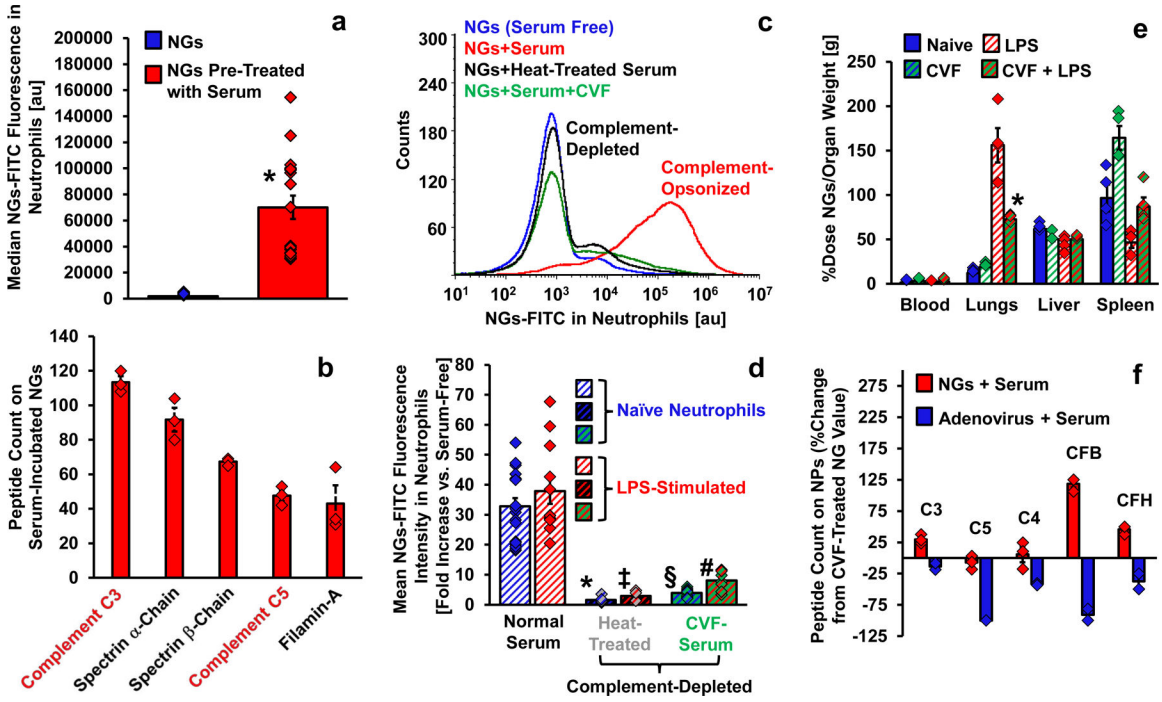

Figure 4. Complement Opsonization of NAPs is Necessary for NAP Uptake in Neutrophils.

(a) Flow cytometry data indicating neutrophils take up lysozyme-dextran nanogels (NGs) after NG incubation in mouse serum (n=18 biological replicates) but not after NG incubation in buffer (n=18 biological replicates, **: $p=6.9\times10^{-9}$*). (b) Mass spectrometry characterization of proteins adsorbed on NGs after incubation with mouse serum as in (a). Plotted data indicates the concentration of detected peptides associated with the five most abundant proteins on serum-incubated NGs (n=3 serum/NG preparations). Complement proteins are highlighted in red text. (c-d) Flow cytometric assessment of NG uptake in mouse neutrophils after NG incubation with; buffer; mouse serum; heat-treated mouse serum and; mouse serum treated with cobra venom factor. Example histograms of NG fluorescence in neutrophils for different serum conditions are depicted in (c). Data reflecting NG mean fluorescence in neutrophils for different serum conditions is plotted in (d). In (d), bars with blue stripes indicate naïve neutrophils (n=18 biological replicates for naïve serum, n=10 for heat-treated serum, n=11 for CVF-treated serum) and bars with red stripes indicate LPS-stimulated neutrophils (n=12 biological replicates for naïve serum, n=5 for heat-treated serum, n=7 for CVF-treated serum). For comparison to normal serum/naïve, **: $p<1\times10^{-10}$* and *§: $p<1\times10^{-10}$*. For comparison to normal serum/LPS, *‡: $p=7.3\times10^{-10}$* and *#: $p=3.7\times10^{-9}$*. (e) Biodistributions of NGs in; naïve mice (n=4 animals); mice treated with CVF (n=4 animals); mice treated with IV LPS (n=4 animals) and; mice treated with IV LPS and CVF (n=4 animals). Naïve and IV-LPS data is identical to that presented in supplementary figure 13, upper right panel. For comparison between LPS and CVF + LPS groups, **: $p=1.6\times10^{-10}$*. (f) Mass spectrometry characterization of complement opsonization of NGs (n=3 serum/NG preparations) and human adenovirus (n=3 serum/adenovirus preparations). Peptide count data as in (b) is normalized to peptide counts on NGs incubated with complement-depleted CVF-treated serum. Relative complement quantities below zero indicate complement opsonization at lower levels than on NGs after treatment with complement-depleted serum.

Statistical significance in (a) is derived from paired two-tailed t-tests. Statistical significance in (d) is derived from one-way ANOVA with Tukey's multiple comparisons test. Statistical significance in (e) is derived from two-way ANOVA with Tukey's multiple comparisons test. All error bars indicate mean ± SEM.

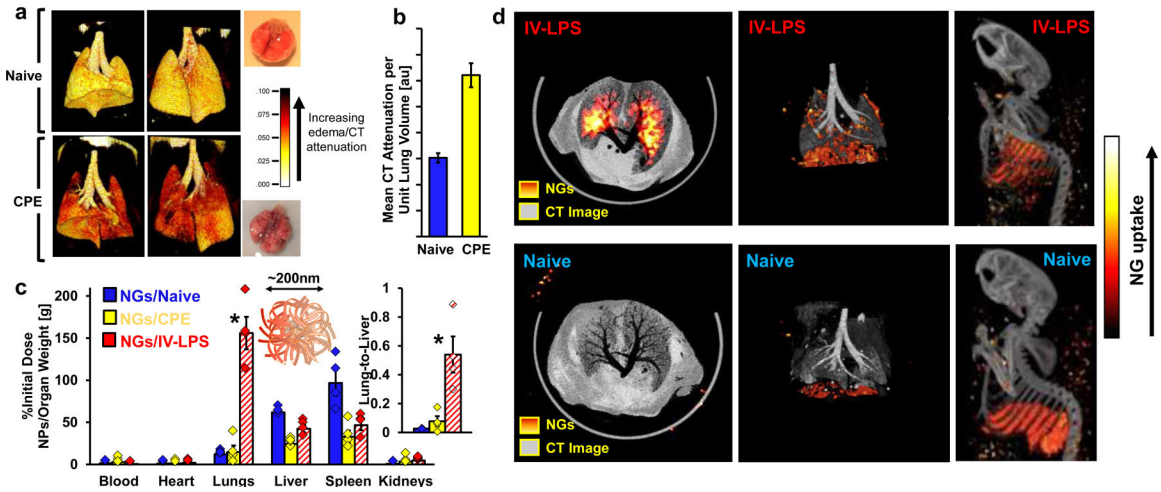

Figure 5. Specificity of NAPs for LPS-Inflamed Lungs vs. Edematous Lungs and SPECT Imaging of NAPs in LPS-Inflamed Lungs.

(a) Three-dimensional reconstructions of chest CT data for naïve mouse lungs and lungs with cardiogenic pulmonary edema (CPE). White/yellow indicates lower attenuation, corresponding to airspace in healthy lungs. Red/dark background indicates higher attenuation, corresponding to fluid in the lungs. (b) Quantification of CT attenuation in naive (blue) and edematous (yellow) lungs, averaged across axial slices (individual slice values in supplementary figure 32). (c) Biodistributions of 200 nm lysozyme-dextran nanogels in naïve mice, mice treated with IV-LPS, and mice subject to cardiogenic pulmonary edema (n=4 animals). Naïve and IV-LPS data is identical to that presented in supplementary figure 13, upper right panel. For comparison of CPE and IV-LPS values, **: $p<1\times10^{-10}$ for main panel and $p=0.005$ for inset*. (d) Co-registered CT (greyscale) and SPECT (red-yellow) images indicating ^{111}In- labeled lysozyme-dextran nanogel uptake in a naïve and an IV-LPS-affected mouse. White/yellow indicates more nanogel uptake. Red/dark background indicates less lysozyme-dextran nanogel uptake. Statistical significance in (c) is derived from two-way ANOVA with Tukey's multiple comparisons test. All error bars indicate mean ± SEM.

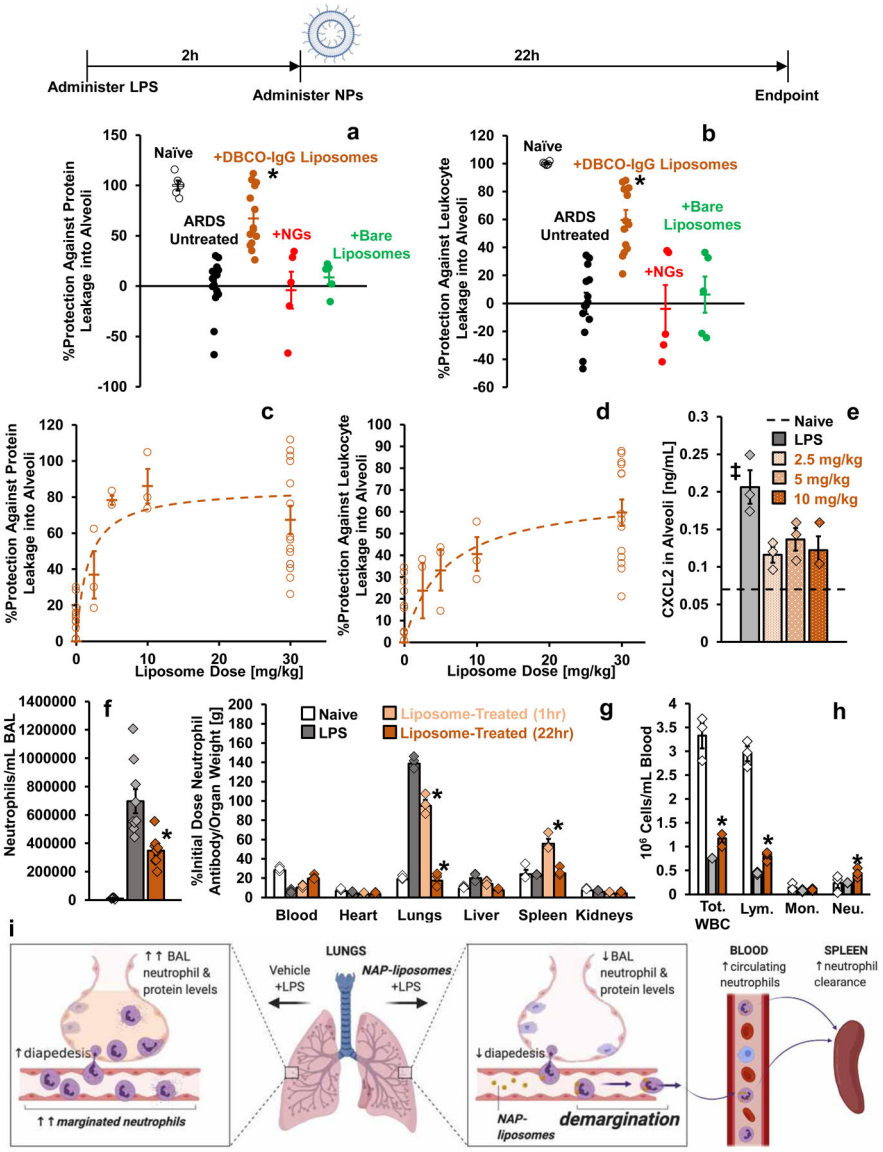

Figure 6. Effects of NAPs in Model Acute Respiratory Distress Syndrome.

Timeline: Nanoparticles or vehicle were administered as an IV bolus two hours after nebulized LPS administration (Liposome schematic created with BioRender.com). (a-b) Bronchoalveolar lavage fluid (BALF) was harvested 22 hours after nanoparticle (30 mg/kg) or vehicle administration. (a) Protein concentration in BALF, reflecting quantity of edema in naïve mice (n=5 animals), sham-treated mice with model ARDS (n=15 animals), and mice with model ARDS treated with DBCO-IgG liposomes (n=14 animals), NGs (n=5 animals), or bare PEGylated liposomes (n=5 animals). **: $p=6.6\times10^{-7}$, 0.0001, and 0.002* for comparison of DBCO-IgG liposome treatment with sham treatment, NG treatment, and bare liposome treatment, respectively. (b) Concentration of leukocytes in BALF for same groups as in (a). **: $p=1.1\times10^{-6}$, 0.0001, and 0.002* for comparison of DBCO-IgG liposome treatment with sham treatment, NG treatment, and bare liposome treatment, respectively. Quantities in (a-b) are represented as degree of protection against infiltration into alveoli,

extrapolated from levels in naïve mice (100% protection) and untreated mice with model ARDS (0% protection). (c-d) Dose-response for edema (c) and leukocyte infiltration (d) in alveoli of ARDS mice treated with DBCO-IgG liposomes. Data were obtained as in (a-b), but with different liposome doses (n=3 animals for 2.5 mg/kg, 5 mg/kg, and 10 mg/kg liposome doses). (e) Chemokine CXCL2 levels in alveoli of LPS-injured mice with and without DBCO-IgG liposome treatment (n=3 animals for all groups). Dashed line indicates CXCL2 levels in alveoli of naïve mice. *‡: p=0.024, 0.079, and 0.034* for comparison of sham treatment with 2.5 mg/kg, 5 mg/kg, and 10 mg/kg DBCO-IgG liposomes treatment, respectively. (f) Concentration of neutrophils in BALF of naïve mice (n=5 animals), mice with model ARDS (n=9 animals), and mice with model ARDS dosed with 30 mg/kg DBCO-IgG liposomes (n=9 animals). For comparison of DBCO-IgG liposome treatment to sham treatment, **: p=0.009*. (g) Biodistributions of anti-Ly6G antibody in naïve mice (n=3 animals), LPS-injured mice (n=3 animals), and mice treated with 10 mg/kg DBCO-IgG liposomes, with organs sampled at 1 hour after treatment (n=3 animals) or 22 hours after treatment (n=3 animals). Naïve and untreated LPS-affected data are identical to data in supplementary figure 1a. **: $p<1\times10^{-10}$* for all comparisons of anti-Ly6G uptake in lungs or spleen of liposome-treated mice vs. sham treated mice. (h) Complete blood count analysis of circulating leukocyte concentrations in naïve mice (n=3 animals), LPS-injured mice (n=3 animals), and mice treated with 10 mg/kg DBCO-IgG liposomes, with blood sampled 22 hours after treatment (n=3 animals). **: p=0.019, 0.025, and 0.047* for comparison of DBCO-IgG liposome-treated to sham-treated values for total white blood cell, lymphocyte, and neutrophil counts, respectively. (i) Schematic for the fate of neutrophils in mice with model ARDS, with and without DBCO-IgG liposome treatment, based on data in (f-h) (created with BioRender.com). Statistical significance in (a), (b), (e), and (f) is derived from one-way ANOVA with Tukey's multiple comparisons test. Statistical significance in (g-h) is derived from two-way ANOVA with Tukey's multiple comparisons test. All error bars indicate mean ± SEM.